Optical Materials 142 (2023) 114036

Contents lists available at ScienceDirect

Optical Materials

journal homepage: www.elsevier.com/locate/optmat

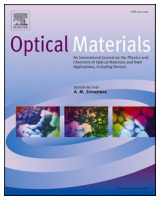

Research Article

Manganese-doped zinc germanate phosphors with vivid luminescent properties for anti-counterfeit applications

Zishen Yang [a], Levi D. Spencer [a], Delaney R. Patocka [a,b], Anjaneyulu Putta [a], Erin E. Schnetzer [a], Jon Kellar [c], Chaoyang Jiang [a,*]

[a] Department of Chemistry and Center for Fluorinated Functional Materials, University of South Dakota, Vermillion, SD, 57069, USA
[b] Department of Natural Science, Peru State College, Peru, NE, 68421, USA
[c] Department of Materials and Metallurgical Engineering and Center for Understanding and Disrupting the Illicit Economy, South Dakota School of Mines and Technology, Rapid City, SD, 57701, USA

ARTICLE INFO

Keywords:
Photostimulated luminescence
Solid-state synthesis
Anti-counterfeiting
Persistent luminescence
Mn doped zinc germanate

ABSTRACT

Fluorescent materials are commonly used in optical labels for anti-counterfeiting purposes. However, these well-known materials can be vulnerable to forgery. It is thus essential to develop new types of luminescent materials with unique optical properties. In this paper, we prepared metal-doped phosphor materials with an inorganic matrix using a high temperature solid-state reaction. The synthesized Mn-doped zinc germanate (ZGO:Mn) phosphors were characterized using various techniques, such as X-ray powder diffraction and photoluminescence spectroscopy, in order to understand their structural and optical properties. The ZGO:Mn phosphors exhibit green color fluorescence, persistent luminescence, and photostimulated luminescence (PSL), which are ideal for anti-counterfeiting applications. Several examples of using the PSL active materials on various substrates demonstrate their capability to prevent counterfeiting and forgery. We further showed that an iPhone can be used to reveal the ZGO:Mn-based security labels. This study contributes to the exploration of novel security materials and offers practical implications for the development of security and authentication technologies.

1. Introduction

Counterfeit goods are a widespread problem in many aspects of daily life, such as passports and driver licenses and even medical drugs and clothing. Counterfeit products are usually of inadequate quality, have less or no efficiency, and can be associated with other illegal activities. To combat counterfeiters, manufacturers implement a variety of anti-counterfeiting strategies in their products, such as water marks, [1] microprinting patterns, [2] holographs, [3] security labels, [4] and quick response (QR) codes. [5,6] More recently, researchers have explored novel functional materials with unique properties, such as persistent luminescence, thermochromism, photochromism, [7,8] and surface enhanced Raman scattering (SERS), [9,10] which can be assembled or deposited in desired patterns to increase the security levels and encoding capacity of anti-counterfeit labels. For example, Ye et al. designed anti-counterfeit labels with physically unclonable functions (PUFs) using SERS-active core-shell nanoparticles. [7,11] May and co-workers printed QR codes using lanthanide-doped upconversion nanoparticles with either visible or near infrared emissions. [12–14] These new approaches are effective, have high storage capacity, are easily recognizable, and are often sufficiently complex to make counterfeiting difficult.

Luminescent materials are broadly utilized in making unique labels for the purpose of anti-counterfeiting due to their intrinsic properties, including versatile types of active materials, easy characterize and process, capable of visual recognition, and convenient for on-site detection. New luminescent materials, such as carbon dots, [15] quantum dots, [16] polymer dots, [17] and lanthanide-based crystals, [18] have been studied for security applications. While most research is focused on emissions in the visible region, there are also reports that attempt to use near infrared (NIR) emission for anti-counterfeiting. In many cases, visual inspections are sufficient in label recognition. Colorful texts, vivid figures and patterns can make an anti-counterfeiting technique very convenient and user-friendly. So far, several types of luminescence have been used in fabricating novel anti-counterfeiting labels, including phosphorescence/persistent luminescence (PersL),

Abbreviations: ZGO, zinc germanate; PSL, photostimulated luminescence.

* Corresponding author.
E-mail address: CY.Jiang@usd.edu (C. Jiang).

https://doi.org/10.1016/j.optmat.2023.114036
Received 2 May 2023; Received in revised form 8 June 2023; Accepted 12 June 2023

[19,20] circularly polarized luminescence (CPL), [21] upconversion luminescence (UCL), [22] and photostimulated luminescence (PSL). [23]

In principle, PSL is more sensitive than UCL, since a low-energy stimulation is needed to liberate a pre-charged molecule from a trap state to an excited state, which will have radiative relaxations that cause emissions. [24,25]There is an increasing interest in using PSL materials in the field of anti-counterfeiting in recent years. [26–36] In these studies, PSL materials usually contain emitting ions doped in a desired inorganic matrix. Various host materials have been explored, including silicate, [26,27] aluminate, [28] gallate, [29,30] germanate, [31,32] gallogermanate [33,34,37] and others. [35,36] While rare-earth elements are widely used as dopants, there are a few reports that use other metal ions as emitting centers in PSL materials. [30,32,34,38] Overall, there are continued efforts in developing novel PSL materials that have a trap state with a suitable energy that is deep enough to avoid thermoluminescence but shallow enough to allow liberation by low-energy photons, such as near infrared light.

Zinc germanate (Zn_2GeO_4, ZGO) is a promising ternary oxide material that has many practical applications, such as photocatalysis, [39] supercapacitors, [40] batteries, [41] anti-microbials, [42] and electroluminescent devices. [43] ZGO is highly stable and has a band gap of 4.68 eV. Recently, there is an increasing interest in using ZGO as a host material in which a dopant can have unique luminescence properties under UV or near-UV radiation. Manganese-doped Zn_2GeO_4 material (ZGO:Mn) has demonstrated intense green emission at 530 nm upon 254 nm excitation. [38] This emission is associated with the dopant Mn^{2+} color centers which replace the tetrahedral Zn^{2+} sites in the crystal. Furthermore, ZGO:Mn is known to have green persistent luminescence that is suitable for bioimaging. [44] Recently, there have been reports on using ZGO:Mn materials as a luminescent phosphor for information encryption and anti-counterfeiting purposes. For example, Gao and co-worker used lithium as a co-dopant in ZGO:Mn and printed anti-counterfeiting patterns with their multicolor phosphors. [45] To further the development of new security inks, it is essential to have a better understanding of the luminescent behavior of ZGO:Mn phosphor and to explore new methods for integrating ZGO:Mn in anti-counterfeiting labels. In this paper, we synthesized ZGO:Mn phosphors via a solid-state reaction. With the optimization of the synthetic procedure, ZGO:Mn was applied to various substrates to make anti-counterfeiting patterns and their luminescence was examined. In particular, the PSL property of ZGO:Mn was systematically studied. Furthermore, we used a smart phone to check the PSL effectiveness of the ZGO:Mn phosphor, which can be valuable in developing feasible and high-level anti-counterfeiting technologies.

2. Experimental

2.1. Chemicals and materials

ZnO (nanopowder) and GeO_2 (99.999%) were purchased from Millipore Sigma. MnO_2 (99.6%) was purchased from Fisher Scientific. Rhodamine 6G (R6G) was purchased from Acros Organics. Commercially available acrylic and glycerol were used as medium for anti-counterfeiting paint. All chemicals and materials were used without further purification.

2.2. Synthesis and materials process

ZnO, GeO_2, and MnO_2 were weighed out stoichiometrically, and were mixed and ground using an agate mortar and pestle. The mixture was transferred into a porcelain crucible and heated in a muffle furnace (Thermolyne 46900) at 1100 °C for the desired period of time. After the reaction, the products were cooled down naturally and ground again. The phosphor materials were compressed into tablets using a Carver Manual pellet press. To fabricate anti-counterfeiting labels, the phosphor materials (10 wt%) were mixed with acrylic or glycerol solution and painted or casted onto various substrates.

2.3. Characterizations

The phosphor samples were examined with powder X-Ray diffraction (Rigaku Ultima IV). The fluorescence spectra were acquired with a Horiba Fluoromax-4 Spectrofluorometer. For PersL and PSL experiments, the samples were pre-irradiated with 254 nm UV light for 60 s. A commercially available LED NIR source (940 nm 12VDC/300 mA) was used to stimulate the luminescence of phosphor material. The optical images were captured using an iPhone 12 with an NIR filter attached.

3. Results and discussion

The ZGO:Mn materials appear as white powder at room temperature. As shown in Fig. 1a, the powder emits an intense bluish-green fluorescence under UV (254 nm) illumination. A similar color phosphorescence persists after the UV excitation. The photo in Fig. 1a(III) is slightly blurred since such phosphorescence can be better observed in a dark environment. We found that the bluish emission can be significantly enhanced when shining a NIR (940 nm) light on the ZGO:Mn materials, a process called photostimulated luminescence. The color of the PSL emission is slightly bluer as compared to the fluorescence. The spectra of these FL, PL, and PSL emissions are shown in Fig. 1b. The FL has a major emission peak at 534 nm with a width of 50 nm. There are some very weak emissions at shorter wavelengths (below 480 nm). The PersL spectrum is rather simple and has just one emission band center at 534 nm with peak width of 42 nm (FWHM). Similarly, the PSL emission spectrum is centered at 534 nm with a comparable band broadening. Fig. 1c gives the intensities of the FL, PersL, and PSL emissions. Out of the three emissions, the FL intensity is strongest while the PL is two-orders of magnitude lower. It is worth noting that the PSL emission is over 20 times stronger than the PersL, which makes it easily observable by the naked eye. Fig. 1d shows the color of the three emissions in the CIE plot, which are mainly located in the region of bluish green. There are only slight differences among the emissions, indicating that these three luminescence processes may involve the same radiactive relaxation step.

The reaction time and temperature play an essential role in determining the crystal structure and phase purity of the final product when synthesizing ZGO:Mn materials via the high temperature solid state reaction, which, in turn, will affect the luminescence properties for the PSL materials. The crystal structure of ZGO is shown in Fig. 2a, which was recreated with the material data from Materials Project. [46] In this work, XRD was first used to study the crystal structures of ZGO:Mn powders. XRD patterns of ZGO:Mn with various reaction times were shown in Fig. 2b, together with library data for ZnO and GeO_2 raw materials (PDF # 00-080-0075 and PDF #00-036-1463, respectively). After a 30-min reaction at 1100 °C, there are still no noticeable XRD peaks for the ZGO product. For the 1-h reaction sample, new peaks at 21.6, 24.99, 30.8, 33.3 and 37.95° are clearly observed, which is consistent to the library data for ZGO (PDF # 00-011-0687). Meanwhile, the intensities of peaks for both ZnO and GeO_2 reactants decreased. With a longer reaction time, the XRD patterns give stronger ZGO peaks and weaker ZnO and GeO_2 peaks. While the tiny peaks of ZnO and GeO_2 are still visible for the 8-h sample, they disappear in the XRD pattern of the 20-h sample. More importantly, the XRD pattern of the 20-h sample is rather clean and matches very close to the library data of Zn_2GeO_4 without any noticeable crystalline impurities. Similarly, the SEM result (Fig. S1) showed uniform crystallinities. Our results indicate that all the reactants are reacted after a 20-h reaction at 1100 °C, and this solid-state reaction is likely completed. Since the Mn dopant is kept at a very low level (1%), we did not notice any structural difference (peak shift) between the ZGO:Mn and ZGO materials.

The study of XRD patterns of our solid-state synthesis at various

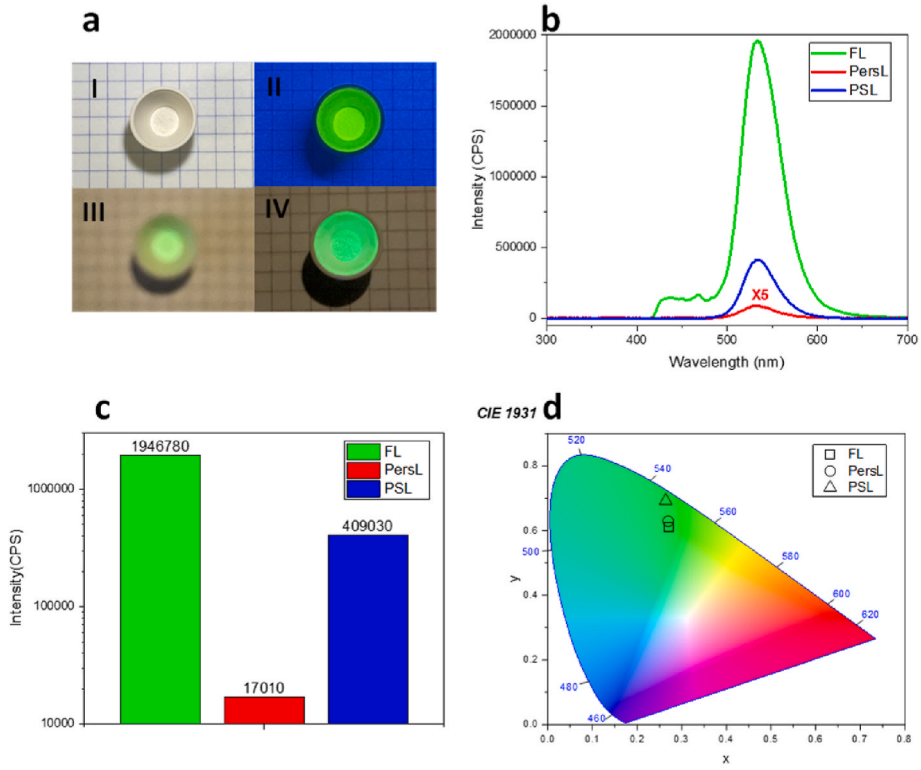

Fig. 1. (a) Optical images of phosphor material under (I) room light, (II) 254 nm UV, (III) afterglow, (IV) 940 nm stimulation; (b) fluorescence spectra of phosphor; (c) intensity comparison of FL, PersL and PSL; (d) CIE plot of FL, PersL and PSL for ZGO:Mn phosphor.

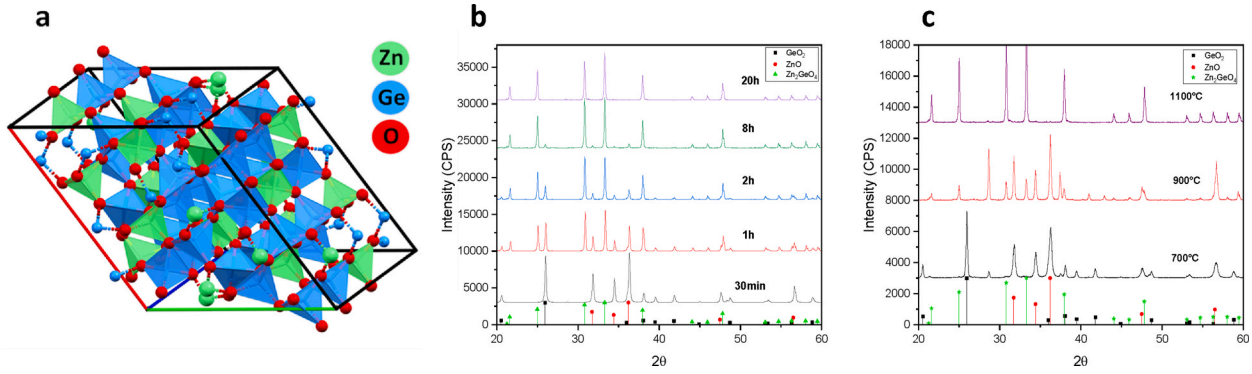

Fig. 2. (a) Crystal structure of Zn_2GeO_4, recreated from Materials Data on Zn_2GeO_4 by Materials Project; Powder XRD pattern of Zn_2GeO_4: Mn under the conditions (b) 1100 °C with different time; and (c) heating for 20 h at different temperatures.

temperatures also provides interesting information. We conducted the synthesis reactions at 700, 900 and 1100 °C for 20-h each. As shown in Fig. 2c, the sample obtained at 700 °C gives an XRD pattern for a mixture of ZnO and GeO_2, indicating that there is no reaction occurring. For the 900 °C, the XRD peaks for GeO_2 have totally disappeared, the ZnO peaks show little changes, and the ZGO peaks appear with weak intensities. There are some new peaks observed in the XRD pattern for this sample, which belong to either reactants or product. This is due to the existence of polymorphs for the GeO_2 crystals. It is found that those peaks, at 28.68, 37.5, and 56.8°, can be assigned to tetragonal GeO_2. From this, we conclude that all hexagonal GeO_2 is converted to a more stable form of tetragonal GeO_2 at 900 °C. Our results are consistent with other reports in the literature. [47] At an even higher temperature (1100 °C), the reaction is completed with all the reactants, including the more stable GeO_2, are converted into the final product, which gives a clean XRD pattern of ZGO powder.

The kinetics of the luminescence of various ZGO:Mn powder were explored. Fig. 3a shows the intensity decay of PersL emission at 534 nm, which can be mathematically fit using a typical decay equation with at least two $t_{1/2}$ values ($t_1 = 13$ ms and $t_2 = 1.2$ s). The decrease in PersL emission can be clearly observed in the dark room. After a strong PersL right after the turn off the UV lamp, the phosphorescence of ZGO:Mn powder persists for a relatively long time (more than 5 min). Fig. 3b demonstrates the enhancement of emission upon NIR stimulation (at 10 s). Here, the PSL decay has $t_{1/2}$ values of 16 ms and 1.8 s. These time constants are slightly greater than that of PersL, indicating an accelerated process of emission due to NIR stimulation. In Fig. 3c, we present experimental data when NIR stimulation was applied intermittently. Each time, turning on the NIR light resulted in a "jump" of emission intensity. When the NIR light was turned off, the emission changed back to an intensity similar to that of a PersL decay. We found that the emission enhancement is 15.36 ± 3.9, with the enhancement decreasing as time goes on (Fig. 1c). There is also a decay process of photo-stimulated phosphorescence luminescence (PSPL). As shown in

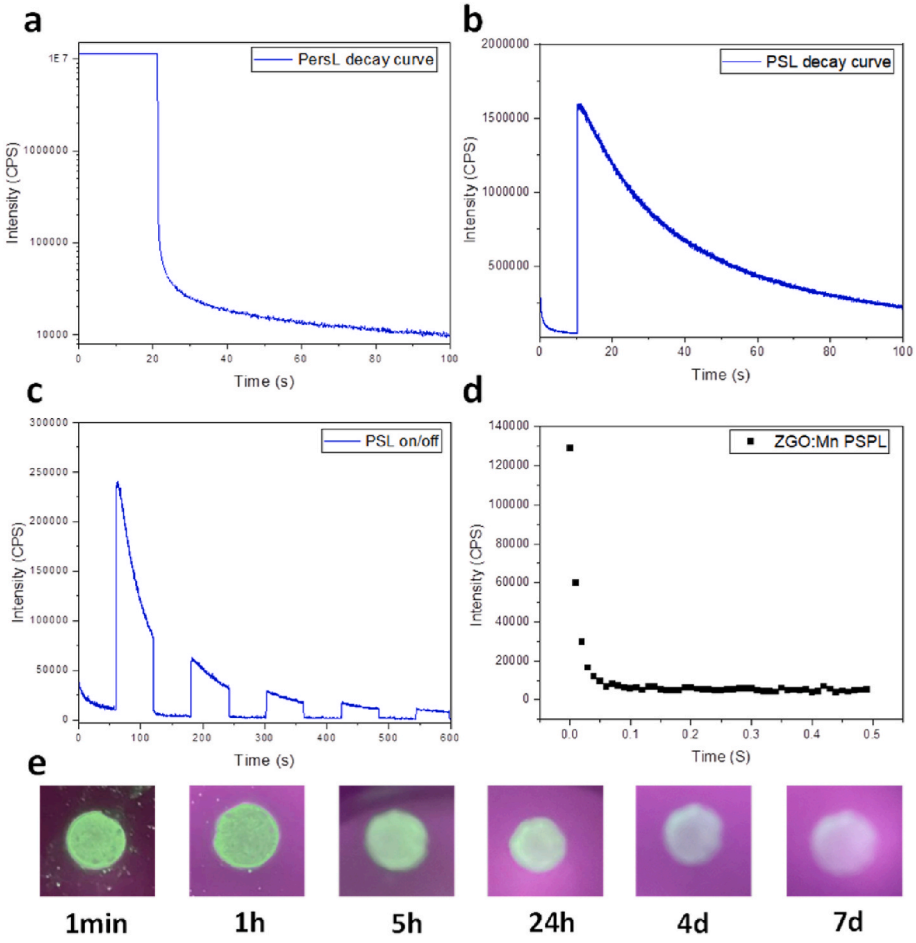

Fig. 3. (a) Decay curve of PersL; (b) decay curve of PSL; (c) PSL on/off experiment; (d) decay curve of PSPL; (e) PSL lifetime monitored at −15 °C.

Fig. 3d, the emission intensity gradually decreased when the NIR stimulation turned off. PSPL decays very fast (the $t_{1/2}$ is found about 12 ms).

PSL of ZGO:Mn powder can be impacted by many external conditions, such as ambient light and temperature. We found that the PSL can still be observed on a ZGO:Mn sample after an extended period if the sample was kept in dark after undergoing a charging process (illuminated by a UV lamp). We also studied the impact of temperature on PSL behavior. One ZGO sample was refrigerated at −15 °C, and its PSL behavior was monitored for a week (see Fig. 3e). We found that the ZGO:Mn sample can be PSL active even after seven days, while the room temperature stored sample has much a shorter PSL active time (less than one day).

Dopant concentration plays an essential role in the optical performances of ZGO:Mn phosphor. We found that increasing the dopant concentration can provide stronger PSL performance when the dopant concentration is below 1.0%. Further increase of the dopant concentration can result in a poor PSL performance (Fig. S2). Such dopant-dependent phenomenon agrees with the work reported by Cui et al., [48] who published that fluorescence intensity decreases when the concentration of Mn^{2+} dopant exceeds 2%, which is due to the concentration quenching effect at a high dopant concentration. [49]

The interesting optical properties, including fluorescence, persistent luminescence, and photostimulated luminescence, in the Mn-doped ZGO materials can be explained by the manganese electronic structures in the ZGO matrix (Fig. 4). It has been reported that ZGO is a semiconductor with a band gap of 4.68 eV. When the ZGO:Mn material is excited by 254 nm UV light, electrons in the valence band are excited to the conduction band. The excited electrons migrate to the excited states of Mn-dopant ions. Some of the electrons will then relax to the $^6A_1$ singlet state

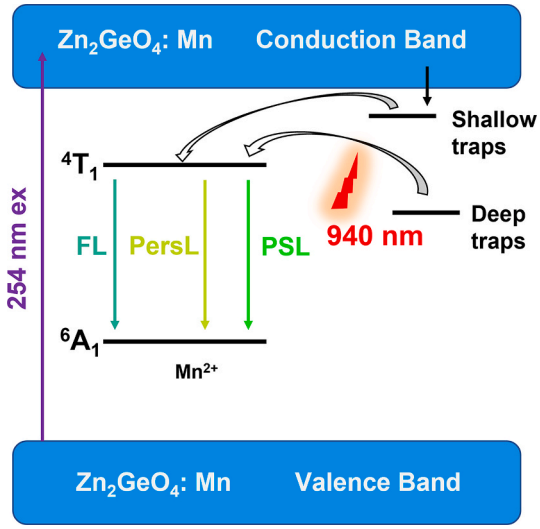

Fig. 4. Schematic representation of the mechanism of FL, PersL, and PSL.

and emit fluorescence. Other electrons may be trapped into the trap states. Those electrons might be "lifted" by thermal energy and then relaxed to ground state, emitting persistent luminescence. Such afterglow could be significantly enhanced by either temperature or radiation, which are known as thermal-stimulated luminescence and photostimulated luminescence, respectively. In our case, NIR light (940 nm) will stimulate the electrons in the trap states (potentially deep trap

states) and then emit light. With such PSL mechanism, it is essential to provide relatively stable trap states for a strong PSL behavior. The Mn-doped ZGO material has a strong PSL emission, which may be due to multiple factors, including the low phonon-vibration of the ZGO matrix, the suitable bandgap of the ZGO materials, the chemical inert of ZGO matrix, multi-electronic states of Mn dopant, and the excellent structural match between the Mn dopant and ZGO matrix.

PSL-active ZGO:Mn powder was explored in the field of anti-counterfeiting labels due to its interesting optical performance. For example, we prepared dot arrays using a laser engraving on a plastic card, and then deposited some ZGO:Mn materials to certain dots with drop casting. As shown in Fig. 5a, the existence of ZGO:Mn materials on the laser engraved card is quite inconspicuous. The designed information, the number 37 in this case, is easily revealed under UV irradiation in ambient condition (Fig. 5b). The green emission can also be observed as PersL when the UV lamp is turned off (Fig. 5c). Additionally, this security label is very sensitive to NIR stimulation. Under 940 nm NIR light, the label can emit stronger green emission than that of PersL (Fig. 5d). Considering various emission modes, this covert label will have three layers of security features with FL, PersL, PSL, respectively. Similarly, we mixed ZGO:Mn with commercially available acrylic paint and successfully painted it on various materials such as plastics, paper, glass, and metal sheets (Figs. S3 and S4). As shown in the Supporting Information, the abbreviation of the University of South Dakota (USD) can be painted “colorlessly” on paper and readily revealed in FL, PersL, and PSL conditions, respectively.

There are several approaches for combining normal organic fluorescent compounds with ZGO:Mn powders to create more complicated anti-counterfeiting materials. Inspired by the well-known Förster resonance energy transfer (FRET) theory, we mixed ZGO:Mn powder with a small portion of Rhodamine 6G (R6G) and studied the optical behavior of the mixture. R6G was chosen since it can absorb the green light from the PSL emission, and then emit a red luminescence around 630 nm. Fig. 6a insert shows a photo of fluorescence for two compressed tablets (ZGO:Mn and its mixture with R6G). We found that the fluorescence of the mixed tablet is greenish yellow with a much dimmer intensity than that of the pure ZGO:Mn tablet. In the fluorescence spectrum, a new peak at 615 nm emerged, which is associated with the fluorescence emission of the R6G (Fig. 6a). The coordinates of the fluorescence emission in the CIE plot are (0.28, 0.42), which is very different to the ZGO:Mn emission (0.27, 0.61). Similarly, the PSL emission from the mixed tablet is also much dimmer and the color also varies.

We also tried using both ZGO:Mn material and other fluorescent dyes to make anti-counterfeiting labels with multilayer security features. Fig. 7a shows a dot array on a plastic card that have been deposited with ZGO:Mn material and fluorescein dye. The symbol of a checkmark can be seen under ambient light due to the red color of fluorescein. Under the UV irradiation, the pattern changes into a yellowish checkmark in a green square box (Fig. 7b). As soon as the UV-lamp was removed, the checkmark disappeared while the square box is still visible due to the PersL of ZGO:Mn material. This square box with the ZGO:Mn materials will be even brighter (more intense green emission) upon the NIR stimulation (Fig. 7c). In this experiment, multiple security features were implemented using a combination of usual organic dye and the novel PSL materials, including the response in various optical condition and changes of emission pattern, color, and intensities.

PSL-active ZGO:Mn materials have a strong green emission under a NIR stimulation, which makes it possible to prepare anti-counterfeiting labels that are sensitive to a NIR light. Nowadays, the smart phone is a ubiquitous device and NIR emission is used for various functions such as face recognition. We studied the PSL of ZGO:Mn materials with a NIR source on an iPhone 13 Pro. As shown in Fig. 7d, a picture of a dinosaur and a meteorite was drawn. The dinosaur is not readily apparent as it is drawn with the previously mentioned paint of ZGO:Mn powder in colorless acrylic. The meteorite is in a red color since R6G was mixed in the paint. Under the UV lamp, the green dinosaur and yellow meteorite were observed. The intensities of PersL are much weaker. We found that the green dinosaur can be clearly observed when the NIR light of an iPhone was turned on by an app for face-recognition (see Fig. 7f). Our results showed that even a simple drawing can produce multiple levels of security features. In addition, using an iPhone as an NIR source could be very convenient for the general public when examining an anti-counterfeiting label in an authentication process.

4. Conclusions

In summary, we have successfully synthesized metal-doped phosphor materials, Mn-doped zinc germanate, using a simple high-temperature solid-state reaction, and characterized them using X-ray diffraction and photoluminescence spectroscopy. These ZGO:Mn

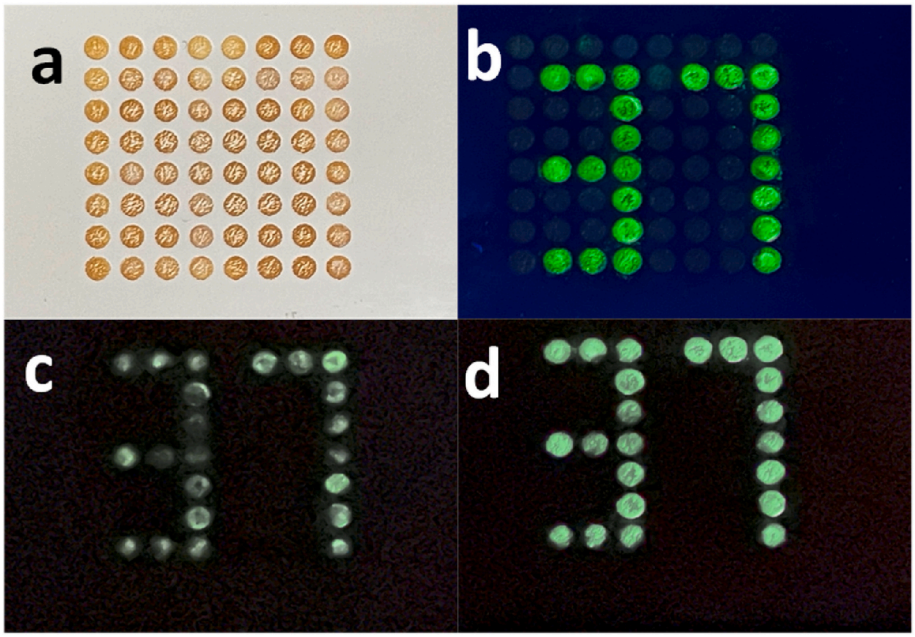

Fig. 5. Optical images of hidden information card under (a) room light, (b) 254 nm UV, (c) afterglow, (d) 940 nm stimulation.

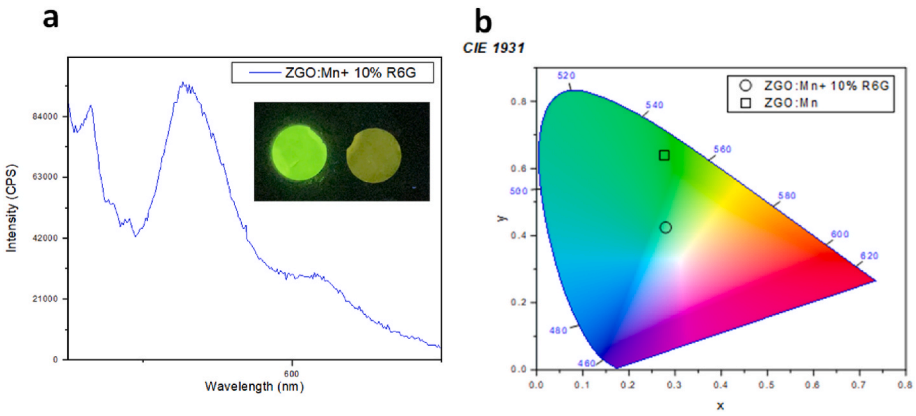

Fig. 6. (a) fluorescence spectrum of phosphor with added R6G; Insert: optical image of neat phosphor pellet (left) and phosphor with added R6G pellet (right); (b) CIE plot of the neat phosphor and phosphor with added R6G.

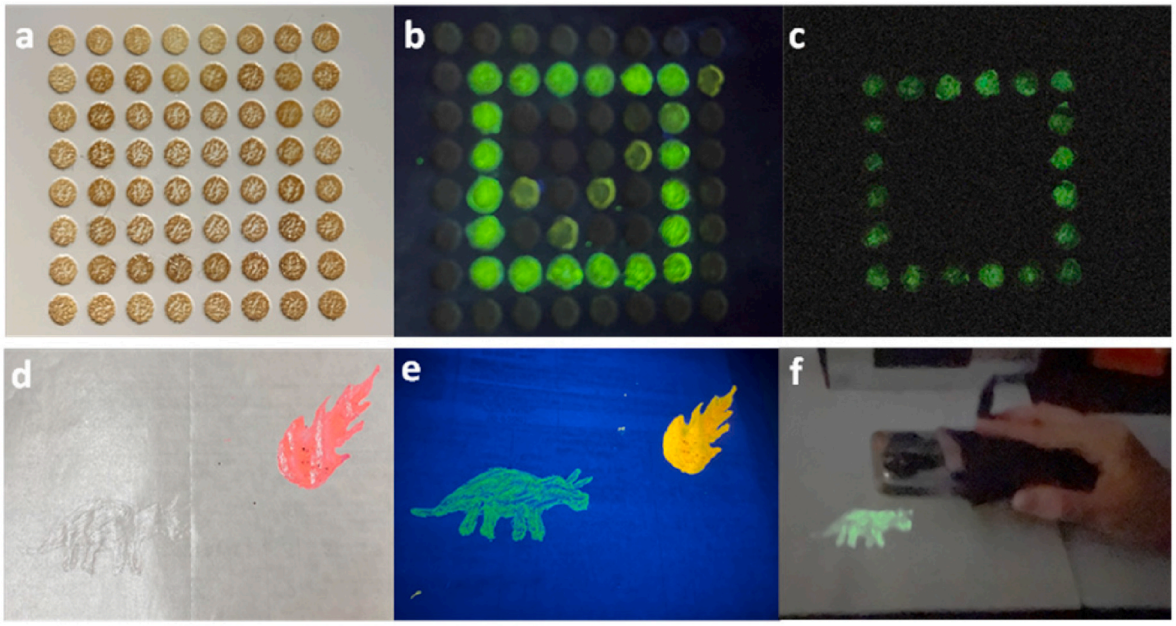

Fig. 7. Optical images of multilayer security card under (a) room light, (b) 254 nm UV lamp, and (c) 940 nm stimulation. Duo color patterns under (d) room light; (e) 254 nm UV lamp; and (f) demonstration of anti-counterfeiting using iPhone 13 Pro.

phosphors possess stable green fluorescence and PersL emission with a peak maximum at 534 nm. In addition, photostimulated luminescence was observed when the UV illuminated phosphors was stimulated using a NIR light. Examples of using PSL-active materials were demonstrated on various substrates to prevent counterfeiting and forgery. Moreover, our results indicated that the ZGO:Mn based security patterns can be easily revealed using a smart phone. Our work contributes to the advancement of security materials and may lead to the creation of more sophisticated anti-counterfeiting technologies.

CRediT authorship contribution statement

Zishen Yang: Conceptualization, Methodology, Validation, Investigation, Writing – original draft, Writing – review & editing. **Levi D. Spencer:** Validation, Formal analysis, Investigation, Writing – review & editing. **Delaney R. Patocka:** Methodology, Investigation. **Anjaneyulu Putta:** Investigation, Writing – review & editing. **Erin E. Schnetzer:** Validation, Investigation, Writing – review & editing. **Jon Kellar:** Conceptualization, Resources, Writing – review & editing. **Chaoyang Jiang:** Conceptualization, Methodology, Writing – original draft, Writing – review & editing, Supervision.

Declaration of competing interest

The authors declare that they have no known competing financial interests or personal relationships that could have appeared to influence the work reported in this paper.

Data availability

Data will be made available on request.

Acknowledgements

This work is funded by the South Dakota Governor's Office of Economic Development through the Governor's Research Center for Understanding and Disrupting the Illicit Economy. DP thanks the support from the NSF REU grant (EEC-1852306). ES thanks the support from the NSF NRT grant (DGE-1828288).

Appendix A. Supplementary data

Supplementary data to this article can be found online at https://doi.org/10.1016/j.optmat.2023.114036.

References

[1] X.W. Yu, H.Y. Zhang, J.H. Yu, Aggregate 2 (1) (2021) 20.
[2] J. Jang, H. Jeong, G.W. Hu, C.W. Qiu, K.T. Nam, J. Rho, Adv. Opt. Mater. 7 (4) (2019), 1801070.
[3] S.C. Fu, Y.C. Liu, L. Dong, Z.F. Lu, W.L. Hu, M.G. Xie, Mater. Lett. 59 (11) (2005) 1449.
[4] A.K. Singh, S. Singh, B.K. Gupta, ACS Appl. Mater. Interfaces 10 (51) (2018), 44570.
[5] Y.M. Wang, X.T. Tian, H. Zhang, Z.R. Yang, X.B. Yin, ACS Appl. Mater. Interfaces 10 (26) (2018), 22445.
[6] M.L. You, M. Lin, S.R. Wang, X.M. Wang, G. Zhang, Y. Hong, Y.Q. Dong, G.R. Jin, F. Xu, Nanoscale 8 (19) (2016), 10096.
[7] A. Abdollahi, H. Roghani-Mamaqani, B. Razavi, M. Salami-Kalajahi, ACS Nano 14 (11) (2020), 14417.
[8] H. Zhou, J. Han, J. Cuan, Y. Zhou, Chem. Eng. J. 431 (2022), 134170.
[9] Y. Huo, Z. Yang, T. Wilson, C. Jiang, Adv. Mater. Interfac. 9 (17) (2022), 2200201.
[10] Y.J. Sun, D.Y. Lou, W. Liu, Z.K. Zheng, X.D. Chen, Adv. Opt. Mater. (2023), 2201549.
[11] Y.Q. Gu, C. He, Y.Q. Zhang, L. Lin, B.D. Thackray, J. Ye, Nat. Commun. 11 (1) (2020) 516.
[12] J.M. Meruga, W.M. Cross, P.S. May, Q. Luu, G.A. Crawford, J.J. Kellar, Nanotechnology 23 (39) (2012), 395201.
[13] A. Baride, J.M. Meruga, C. Douma, D. Langerman, G. Crawford, J.J. Kellar, W. M. Cross, P.S. May, RSC Adv. 5 (123) (2015), 101338.
[14] J.M. Meruga, W.M. Cross, J.B. Petersen, P.S. May, A. Baride, K. Cessac, J.J. Kellar, Langmuir 34 (4) (2018) 1535.
[15] J. Guo, H. Li, L. Ling, G. Li, R. Cheng, X. Lu, A.-Q. Xie, Q. Li, C.-F. Wang, S. Chen, ACS Sustain. Chem. Eng. 8 (3) (2020) 1566.
[16] S.J. Park, J.Y. Park, J.W. Chung, H.K. Yang, B.K. Moon, S.S. Yi, Chem. Eng. J. 383 (2020), 123200.
[17] W.K. Tsai, Y.S. Lai, P.J. Tseng, C.H. Liao, Y.H. Chan, ACS Appl. Mater. Interfaces 9 (36) (2017), 30918.
[18] Y.L. Liu, K.L. Ai, L.H. Lu, Nanoscale 3 (11) (2011) 4804.
[19] N. Katumo, K. Li, B.S. Richards, I.A. Howard, Sci. Rep. 12 (1) (2022) 2100.
[20] G. Cai, T. Delgado, C. Richard, B. Viana, Materials 16 (3) (2023) 1132.
[21] J.W. Lv, X.K. Yang, Z.Y. Tang, Adv. Mater. 35 (7) (2023), 2209539.
[22] H. Suo, Q. Zhu, X. Zhang, B. Chen, J. Chen, F. Wang, Mater. Today Phys. 21 (2021), 100520.
[23] Y. Fan, X.F. Jin, M.Y. Wang, Y. Gu, J.Y. Zhou, J.C. Zhang, Z.F. Wang, Chem. Eng. J. 393 (2020), 124799.
[24] X.T. Fan, Z.C. Liu, X.X. Yang, W.B. Chen, W. Zeng, S.Y. Tian, X. Yu, J.B. Qiu, X. H. Xu, J. Rare Earths 37 (7) (2019) 679.
[25] L.F. Yuan, Y.H. Jin, Y. Su, H.Y. Wu, Y.H. Hu, S.H. Yang, Laser Photon. Rev. 14 (12) (2020), 2000123.
[26] Z.C. Liu, L. Zhao, W.B. Chen, X.T. Fan, X.X. Yang, S.Y. Tian, X. Yu, J.B. Qiu, X. H. Xu, J. Mater. Chem. C 6 (41) (2018), 11137.
[27] S.S. Peng, L. Liu, L.Z. Wang, R. Rong, L. Song, W.X. You, J.P. Shi, Y. Zhang, J. Rare Earths 40 (9) (2022) 1417.
[28] P.P. Li, Y. Tian, F.F. Huang, L. Lei, M.Z. Cai, S.Q. Xu, J.J. Zhang, J. Eur. Ceram. Soc. 42 (12) (2022) 5065.
[29] S.S. Ding, P.H. Chen, H.J. Guo, P. Feng, Y.P. Zhou, Y.H. Wang, J.L. Sun, J. Energy Chem. 69 (2022) 150.
[30] Y.M. Tang, M.X. Deng, Z.Z. Zhou, J.C. Wang, Q. Liu, J. Am. Ceram. Soc. 105 (10) (2022) 6241.
[31] Z.Y. Sun, J.X. Yang, L.W. Huai, W.X. Wang, Z.D. Ma, J.K. Sang, J.C. Zhang, H.H. Li, Z.P. Ci, Y.H. Wang, ACS Appl. Mater. Interfaces 10 (25) (2018), 21451.
[32] D.L. Gao, K.W. Ma, P. Wang, X.Y. Zhang, Q. Pang, H. Xin, Z.H. Zhang, H. Jiao, Dalton Trans. 51 (2) (2022) 553.
[33] D.L. Gao, J. Gao, F. Gao, Q.Q. Kuang, Y. Pan, Y.F. Chen, Z.W. Pan, J. Mater. Chem. C 9 (46) (2021), 16634.
[34] D.L. Gao, Q.Q. Kuang, F. Gao, H. Xin, S.N. Yun, Y.H. Wang, Mater. Today Phys. 27 (19) (2022), 100765.
[35] Z.H. Lu, J. Tang, P. Du, W.P. Li, Z.F. Liu, J. Wang, L.H. Luo, Ceram. Int. 47 (6) (2021) 8248.
[36] S.L. Tian, P. Feng, S.S. Ding, Y.J. Wang, Y.H. Wang, J. Alloys Compd. 899 (2022), 163325.
[37] D.L. Gao, P. Wang, F. Gao, W. Nguyen, W. Chen, Nanomaterials 12 (12) (2022) 2029.
[38] N.M.C.H.P. Lan, C.X. Thang, N.D.T. Kien, N.V. Tung, Mater. Trans. 63 (2) (2022) 197–202.
[39] J. Huang, X. Wang, Y. Hou, X. Chen, L. Wu, X. Fu, Environ. Sci. Technol. 42 (19) (2008) 7387.
[40] P. Liu, Q. Ru, P. Zheng, Z. Shi, Y. Liu, C. Su, X. Hou, S. Su, F. Chi-Chung Ling, Chem. Eng. J. 374 (2019) 29.
[41] X. Chen, X. Ran, Y. Lu, C. Feng, Ionics 27 (10) (2021) 4177.
[42] J.-H. Gong, L.-J. Chen, X. Zhao, X.-P. Yan, ACS Appl. Mater. Interfaces 14 (15) (2022), 17142.
[43] J.P. Bender, J.F. Wager, J. Kissick, B.L. Clark, D.A. Keszler, J. Lumin. 99 (4) (2002) 311.
[44] R.M. Calderón-Olvera, E. Arroyo, A.M. Jankelow, R. Bashir, E. Valera, M. Ocaña, A. I. Becerro, ACS Appl. Mater. Interfaces (2023), 20613.
[45] D.L. Gao, F. Gao, Q.Q. Kuang, X.Y. Zhang, Z.H. Zhang, Y. Pan, R.P. Chai, H. Jiao, ACS Appl. Nano Mater. 5 (7) (2022) 9929.
[46] P. The Materials, Materials Data on Zn_2GeO_4 by Materials Project, 2020. United States.
[47] A.A. Bolzan, C. Fong, B.J. Kennedy, C.J. Howard, Acta Crystallogr. B 53 (3) (1997) 373.
[48] Z. Cui, G.W. Deng, O.U. Wang, X.L. Luo, Z.H. Li, M. Yang, S.H. Cheng, X.Y. Liu, ChemistrySelect 6 (39) (2021), 10554.
[49] Y.M. Li, S. Qi, P.L. Li, Z.J. Wang, RSC Adv. 7 (61) (2017), 38318.